# A Suitable Controller for Frequency Control of Solar-thermal / Biodiesel / Biomass / Micro-hydro Generation of a Remote Community or Farm with Energy Storage

Ioannis Moschos [1], Constantinos Parisses [1] and Ioannis Mastoras [1]

[1] *Department of Electrical and Computer Engineering, University of Western Macedonia, Karamanli & Ligeris, Kozani 50100, Greece*

**Abstract**

This article addresses the application of a fractional order PDF-(1+PI) controller tuned by the coot optimization algorithm in an isolated microgrid for frequency regulation. The microgrid consists of a biodiesel generator, a biomass combined heat and power, an ORC solar thermal power plant, a micro-hydro turbine generator and a wind turbine generator. In addition, battery storage and fuel cells are considered. The work endeavors to present a potent scheme which could be a model of a community or a farm which minimizes its wastes via bioenergy and effectively synchronize between the generation and demand, while minimizing the frequency deviation. The proposed controller is tested for various real-world scenarios. The results conclude that the fractional order PDF-(1+PI) exhibits better transient response than the PIDF and integer order PDF-(1+PI) controllers.

**Keywords**

Fractional order PDF-(1+PI) controller, bioenergy-based generators, load frequency control, microgrid, coot optimization algorithm

## 1. Introduction

The global power consumption is increasing in contrast to the continuous reduction of conventional energy sources, leading to a shift towards renewable energy sources aiming to reduce the negative impact on the environment. The ever-growing energy demand due to modern lifestyle has been producing harmful wastes for the ecosystem. A sustainable solution could be the use of the generated wastes for the production of renewable bioenergy. Although, the available bioenergy cannot cope with the global power demand, it could be used along with solar, wind power and energy storage in remote communities or farms to meet their demand with green energy, whereas the harmful wastes are reduced.

In [1] a PID controller is tested in an isolated microgrid (MG) with various bioenergy units for frequency and voltage regulation. The authors in [2] have applied a PI controller in an isolated MG, while in [3] a PI controller is used in a system with an organic rankine cycle solar thermal power plant (ORC- STPP) and various storage systems. In [4] a PID controller is optimized using the grasshopper optimization algorithm in an isolated MG comprising of a photovoltaic/biogas/biodiesel generator and energy storage, while in [5] a fuzzy PID controller is used for a MG with energy storage and a thermal power system. Whereas a non-integer sliding mode control is utilized for the frequency regulation of a stand-alone microgrid [6].

The aim of the proposed work is to optimize a fractional order proportional derivative (FO PDF) controller with filter in series with a one plus fractional order proportional integral controller (1+FO PI) via the newly introduced coot optimization algorithm (COA) for the frequency regulation in an isolated MG with various bioenergy units and energy storage, which has the ability to cope with various

Proceedings of HAICTA 2022, September 22–25, 2022, Athens, Greece
EMAIL: mpe00322@uowm.gr (A. 1); kparisis@uowm.gr (A. 2); imastoras@uowm.gr (A. 3)
ORCID: 0000-0002-2918-4830 (A. 1); 0000-0002-2047-9122 (A. 2)


operating conditions. The remainder of the paper is structured as follows. System configuration is presented section 2, followed by an analysis of the COA in section 3. In section 4 the proposed controller is descripted. The Simulation results are presented and discussed in section 5 followed by conclusions in section 6.

## 2. Description of the Microgrid

The proposed isolated microgrid is based on the utilization of sustainable and renewable resources for optimal operation in a community or farm. The schematic of the microgrid is presented in Figure 1. The parameters are presented in the appendix.

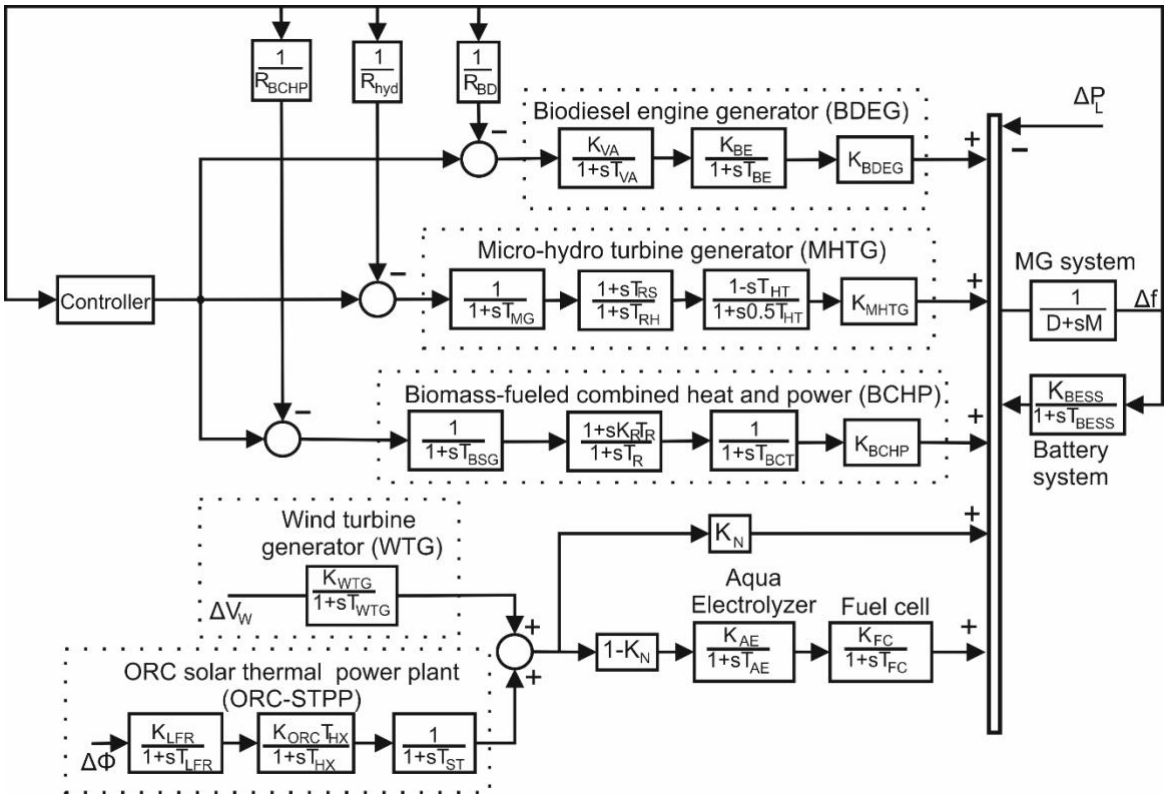


**Figure 1**: Overall scheme of the microgrid for load frequency control

## 3. Coot Optimization Algorithm

The coots are small water birds that are member of the rail family, Rallidae. Based on the behavior of coot's swarm on water Iraj et al [7] introduced a new optimization method, the coot optimization algorithm, which is a swarm-based meta heuristic optimization method.

To achieve their target (food) the coots move behind its front coots in a chain towards a group of leaders who guide the group to their target. The algorithm considers four different moves of coots on the water surface, (1) random movement, (2) Chain movement, (3) Adjusting the position based on the group leaders, (4) Leading the group by the leaders towards the optimal area. The COA starts with a random population and the objective function is repeatedly evaluated for this population until the maximum number of iterations is achieved. The population is randomly generated in the search space using the following expression:

$$CootPos(i) = rand(1, d).* (ub - lb) + lb \quad (1)$$

where $CootPos$ is the coot position, $i$ the coot's index number, d denotes search space dimension $ub$, $lb$ are the upper the lower bounds of the search space. After forming the initial population, the fitness of each coot is determined by calculating the objective function. In the current study the ITAE criterion is considered as the objective function:

$$ITAE = \int_0^{t_{sim}} t|\Delta f(t)|dt \tag{2}$$

Next the four mentioned different movements of the coot's swarm on the water surface are implemented. The random movement is formulated by considering a random position according to formula (3) in the search space and move the coot towards this position.

$$Q = rand(1, d).*(ub - lb) + lb, \tag{3}$$

If the algorithm is trapped in a local optimum the random movement will force the algorithm to escape from the local optimum. The new coot position is calculated by:

$$CootPos(i) = CootPos(i) + A * R2 * \big(Q - CootPos(i)\big), \tag{4}$$

where R2 a random number between 0 and 1, and $A = 1 - iter/Max\_iter$.

In order to implement the chain movement, the average position of two coots is used:

$$CootPos(i) = 0.5\big(CootPos(i-1) + CootPos(i)\big), \tag{5}$$

where the second coot is represented by $CootPos(i-1)$.

The third movement is adjusting the position based on the group leaders. A leader is chosen based on equation (6), where i is the index number of the current coot, NL is the number of leaders and K is the leader's index number.

$$K = 1 + (imodNL) \tag{6}$$

The $coot(i)$ updates its position by applying formula (7), which calculated the next position based on the selected leader.

$$CootPos(i) = LeaderPos(K) + 2 * R1 * \cos(2R\pi) * \big(LeaderPos(K) - CootPos(i)\big), \tag{7}$$

where $LeaderPos(K)$ is the selected leader position, R1 is a random number between 0 and 1 and R is a random number between -1 and 1.

The fourth movement is the leader movement. The group must be directed towards the optimum area, so the leaders need to update their position toward the goal. The leaders update their position based on the following equation:

$$LeaderPos(i) = \begin{cases} B * R3 * \cos(2R\pi) * \big(gBest - LeaderPos(i)\big) + gBest, R4 < 0.5 \\ B * R3 * \cos(2R\pi) * \big(gBest - LeaderPos(i)\big) - gBest, R4 \geq 0.5 \end{cases}, \tag{8}$$

where $gBest$ is the best position ever found, R3 and R4 random number between 0 and 1, R is a random number between -1 and 1 and B is calculated according to $B = 2 - iter/Max\_iter$.

Formula (8) looks for better positions around this current point. $B * R3$ makes larger random movements so that the algorithm does not get stuck in a local optimum, which leads to exploration and exploitation at the same time. Also, $\cos(2R\pi)$ explores around the best search agent with various radius to find a better position around this search agent.

Finally, in order to maintain the random nature of the algorithm, the movements are considered randomly.

## 4. Fractional Calculus and Controller Structure

The fractional calculus is a generalization of the classical integration and differentiation to any real number. In the last years there has been a growing interest in the application of fractional order (FO) controllers in the field of control engineering due to their superior performance in contrast to the integer order (IO) controllers. The most widely used definition is the Caputo definition [8]:

$${}_0D_t^a f(t) = \frac{1}{\Gamma(m-a)} \int_0^t \frac{f^{(m)}(\tau)d\tau}{(t-\tau)^{\alpha+1-m}}, \tag{9}$$

where $m - 1 < a < m, m \in \mathbb{Z}$.

In the current study a FO PDF-(1+PI) is implemented for the load frequency control (LFC) of the proposed microgrid using the COA. The schematic of the controller is depicted in Figure 2.

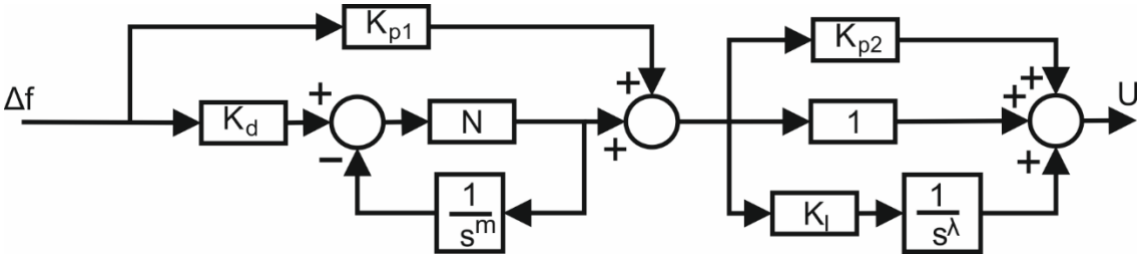


**Figure 2**: Transfer function of the FO PDF-(1+PI) controller

## 5. Simulations

**Table 1**
Optimal controller gains with no solar and wind availability

| PIDF | | | | | | |
|---|---|---|---|---|---|---|
| $K_p$ | | $K_i$ | | $K_d$ | | N |
| 2.844 | | 4 | | 0.2372 | | 485.9112 |
| IO PDF-(1+PI) | | | | | | |
| $K_{p1}$ | | $K_d$ | N | $K_{p2}$ | | $K_i$ |
| 4 | | 1.2652 | 500 | 0.24 | | 4 |
| FO PDF-(1+PI) | | | | | | |
| $K_{p1}$ | $K_d$ | N | $K_{p2}$ | $K_i$ | m | l |
| 3.999 | 0.8263 | 480.194 | 0.4850 | 3.9984 | 1.3057 | 0.8158 |

**Table 2**
Transient response characteristics for non-availability of solar and wind

| Controller | Case 1: $K_{MHTG}$=0.35, $K_{BDEG}$=0.35, $K_{BCHP}$=0.3 | | | |
|---|---|---|---|---|
| | Overshoot | Undershoot | Settling time ($t_s$) | ITAE |
| PIDF | 0.0017 | -0.0854 | 1.9279 | 0.2025 |
| IO PDF-(1+PI) | 0.0279 | -0.0655 | 1.9325 | 0.0585 |
| FO PDF-(1+PI) | 0.0010 | -0.0558 | 0.6993 | 0.0129 |
| | Case 2: $K_{MHTG}$=0.25, $K_{BDEG}$=0.75, $K_{BCHP}$=0 | | | |
| | Overshoot | Undershoot | Settling time ($t_s$) | ITAE |
| PIDF | 0.0055 | -0.0716 | 1.6225 | 0.0746 |
| IO PDF-(1+PI) | 0.0089 | -0.0443 | 0.9205 | 0.0178 |
| FO PDF-(1+PI) | 5.5736e-06 | -0.0332 | 0.6935 | 0.0426 |
| | Case 3: $K_{MHTG}$=0, $K_{BDEG}$=0.9, $K_{BCHP}$=0.1 | | | |
| | Overshoot | Undershoot | Settling time ($t_s$) | ITAE |
| PIDF | 0.0017 | -0.0619 | 1.4986 | 0.0271 |
| IO PDF-(1+PI) | 1.3167e-04 | -0.0325 | 0.6231 | 0.0051 |
| FO PDF-(1+PI) | 0 | -0.0219 | 0.7183 | 0.0519 |
| | Case 4: $K_{MHTG}$=0.2, $K_{BDEG}$=0, $K_{BCHP}$=0.8 | | | |
| | Overshoot | Undershoot | Settling time ($t_s$) | ITAE |
| PIDF | 0.0069 | -0.0883 | 8.9112 | 0.2821 |
| IO PDF-(1+PI) | 0.0109 | -0.0678 | 3.5210 | 0.0655 |
| FO PDF-(1+PI) | 0.0014 | -0.0573 | 0.9222 | 0.0520 |

In this section the simulated results are presented and discussed for the proposed microgrid for various operation and disturbance conditions. In addition, the proposed controller is compared with its

integer counterpart and the classical PID controller with filter. All simulations are performed with Max_iter=50 and N=50.

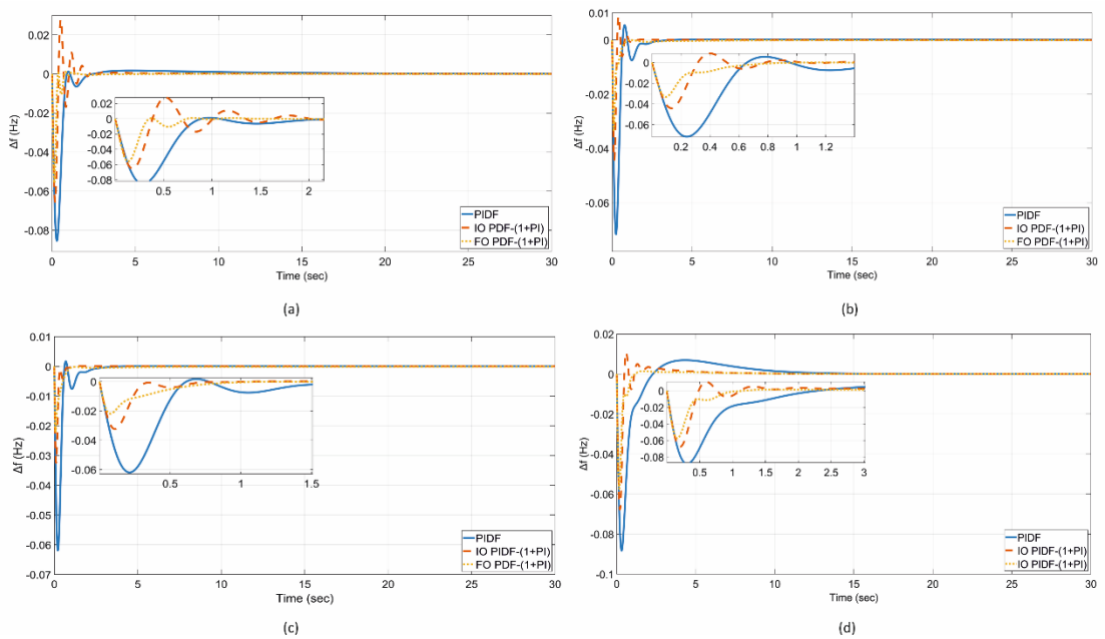


**Figure 3**: Non-availability of solar and wind: (a) Case 1, (b) Case 2, (c) Case 3, (d) Case 4

## 5.1. Frequency Response with No Solar and Wind Availability

This study is carried out considering that there is no solar and wind availability. The proposed controller is optimized for a 10% step load perturbation (SLP) at time 0 s. The optimum controllers' values are presented is Table 1. The transient response characteristics of the system are presented in Table 2 (case 1). In addition, the controllers are tested with various operating conditions: unavailability of BCHP (case 2), MHTG (case 3) and BDEG (case 4) due to maintenance or lack of fuel. Furthermore, the dynamic response of each case is presented in Figure 3. The results reveal that the best performance in each case is achieved by the FO PDF-(1+PI) controller.

## 5.2. Frequency Response with Solar and Wind Availability

**Table 3**
Optimal controller gains with solar and wind availability

| PIDF | | | | | | |
|---|---|---|---|---|---|---|
| $K_p$ | | $K_i$ | | $K_d$ | | N |
| 3.3758 | | 4 | | 0.3818 | | 485.1266 |
| IO PDF-(1+PI) | | | | | | |
| $K_{p1}$ | | $K_d$ | N | $K_{p2}$ | | $K_i$ |
| 4 | | 1.2551 | 500 | 0.2693 | | 4 |
| FO PDF-(1+PI) | | | | | | |
| $K_{p1}$ | $K_d$ | N | $K_{p2}$ | $K_i$ | m | l |
| 3.9994 | 0.7581 | 487.7384 | 0.8758 | 3.9942 | 1.3059 | 0.8155 |

The proposed controller is optimized for a 10% SLP at time 0 s and a constant step change of 1.5% and 2% in the WTG and STPP respectively. The optimum controllers' values are presented is Table 3. The transient response characteristics of the system are presented in Table 4 (case 1). In addition, the controllers are tested with various operating conditions: unavailability of BCHP (case 2), MHTG (case

3) and BDEG (case 4) due to maintenance or ill production of fuel. Furthermore, the dynamic response of each case is presented in Figure 4. The results reveal that the best dynamic response in each case is attained by the FO PDF-(1+PI) controller.

**Table 4**
Transient response characteristics wind solar and wind availability

| Controller | Case 1: $K_{MHTG}$=0.35, $K_{BDEG}$=0.35, $K_{BCHP}$=0.3 | | | |
|---|---|---|---|---|
| | Overshoot | Undershoot | Settling time ($t_s$) | ITAE |
| PIDF | 0.0017 | -0.0806 | 1.7300 | 0.1735 |
| IO PDF-(1+PI) | 0.0290 | -0.0648 | 1.9206 | 0.0523 |
| FO PDF-(1+PI) | 0.0018 | -0.0544 | 0.6345 | 0.0105 |
| | Case 2: $K_{MHTG}$=0.25, $K_{BDEG}$=0.75, $K_{BCHP}$=0 | | | |
| | Overshoot | Undershoot | Settling time ($t_s$) | ITAE |
| PIDF | 0.0032 | -0.0656 | 1.4754 | 0.0636 |
| IO PDF-(1+PI) | 0.0093 | -0.0437 | 0.9437 | 0.0166 |
| FO PDF-(1+PI) | 3.1920e-04 | -0.0315 | 0.6375 | 0.0359 |
| | Case 3: $K_{MHTG}$=0, $K_{BDEG}$=0.9, $K_{BCHP}$=0.1 | | | |
| | Overshoot | Undershoot | Settling time ($t_s$) | ITAE |
| PIDF | 1.3095e-04 | -0.0554 | 1.5774 | 0.0235 |
| IO PDF-(1+PI) | 4.9300e-04 | -0.0321 | 0.5914 | 0.0054 |
| FO PDF-(1+PI) | 4.9977e-05 | -0.0203 | 0.6575 | 0.0437 |
| | Case 4: $K_{MHTG}$=0.2, $K_{BDEG}$=0, $K_{BCHP}$=0.8 | | | |
| | Overshoot | Undershoot | Settling time ($t_s$) | ITAE |
| PIDF | 0.0059 | -0.0836 | 8.6323 | 0.2381 |
| IO PDF-(1+PI) | 0.0125 | -0.0670 | 3.2492 | 0.0576 |
| FO PDF-(1+PI) | 0.0016 | -0.0552 | 0.8327 | 0.0450 |

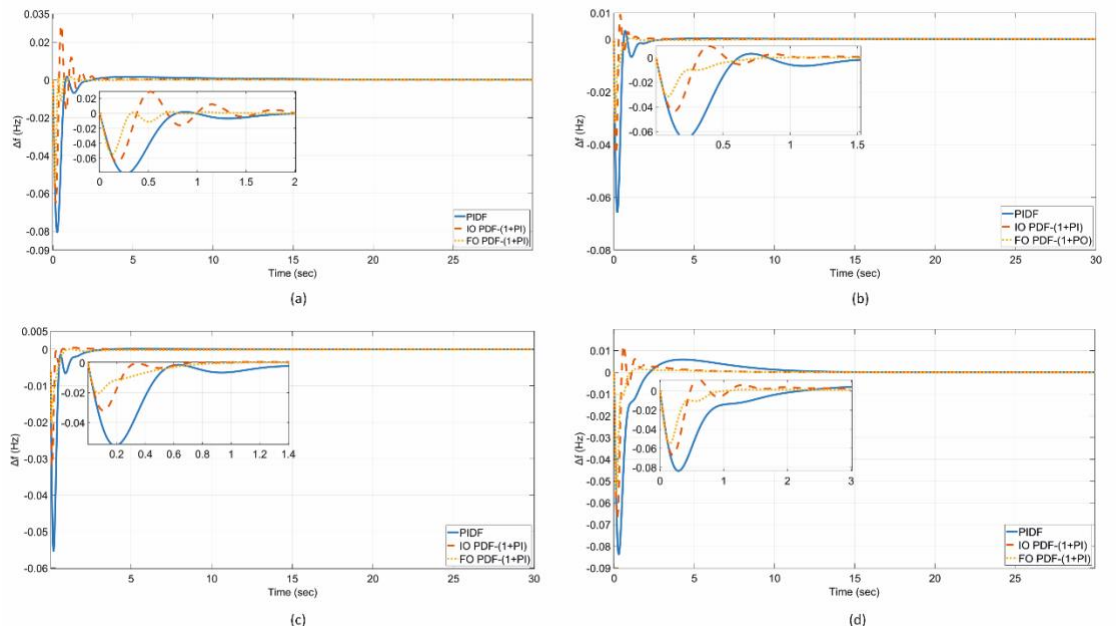


**Figure 4**: Availability of solar and wind: (a) Case 1, (b) Case 2, (c) Case 3, (d) Case 4

## 6. Conclusion

This study has investigated the application of a FO PDF-(1+PI) controller tuned by the coot optimization method in an MG comprising of renewable energy sources and energy storage. The results reveal that the proposed FO PDF-(1+PI) controller exhibits better performance in the case of no STPP and WTG for various operating conditions. When solar and wind power is introduced in the system the proposed controller outperforms the PIDF and IO PDF-(1+PI) controllers in all operating conditions.

Overall, it can be concluded that the proposed controller among the tested controllers is the best solution for the frequency regulation of an isolated MG comprising of bioenergy, hydro, solar, wind generation and energy storage.

## 7. References


[1] A. K. Barik and D. C. Das, "Coordinated regulation of voltage and load frequency in demand response supported biorenewable cogeneration-based isolated hybrid microgrid with quasi-oppositional selfish herd optimisation," *Int. Trans. Electr. Energy Syst.*, vol. 30, no. 1, 2020, doi: 10.1002/2050-7038.12176.

[2] R. Rabeh, M. Ferfra, and A. Ezbakhe, "Secondary control of islanded microgrids using pievolutionary algorithms under uncertainties," *Int. J. Renew. Energy Res.*, vol. 9, no. 4, 2019.

[3] D. C. Das, N. Sinha, and A. K. Roy, "Automatic Generation Control of an Organic Rankine Cycle Solar-Thermal/Wind-Diesel Hybrid Energy System," *Energy Technol.*, vol. 2, no. 8, 2014, doi: 10.1002/ente.201402024.

[4] A. K. Barik and D. C. Das, "Expeditious frequency control of solar photovoltaic/biogas/biodiesel generator based isolated renewable microgrid using grasshopper optimisation algorithm," *IET Renew. Power Gener.*, vol. 12, no. 14, 2018, doi: 10.1049/iet-rpg.2018.5196.

[5] D. K. Lal and A. K. Barisal, "Load Frequency Control of AC Microgrid Interconnected Thermal Power System," *IOP Conf. Ser. Mater. Sci. Eng.*, vol. 225, 2017, doi: 10.1088/1757-899x/225/1/012090.

[6] Z. Esfahani, M. Roohi, M. Gheisarnejad, T. Dragičević, and M. H. Khooban, "Optimal non-integer sliding mode control for frequency regulation in stand-alone modern power grids," *Appl. Sci.*, vol. 9, no. 16, 2019, doi: 10.3390/app9163411.

[7] I. Naruei and F. Keynia, "A new optimization method based on COOT bird natural life model," *Expert Syst. Appl.*, vol. 183, 2021, doi: 10.1016/j.eswa.2021.115352.

[8] I. Podlubny, *Fractional differential equations : an introduction to fractional derivatives, fractional differential equations, to methods of their solution and some of their applications*. 1999.

[9] A. K. Barik and D. C. Das, "Proficient load-frequency regulation of demand response supported bio-renewable cogeneration based hybrid microgrids with quasi-oppositional selfish-herd optimisation," *IET Gener. Transm. Distrib.*, vol. 13, no. 13, 2019, doi: 10.1049/iet-gtd.2019.0166.

[10] Y. Arya *et al.*, "Cascade-IλDμN controller design for AGC of thermal and hydro-thermal power systems integrated with renewable energy sources," *IET Renew. Power Gener.*, vol. 15, no. 3, 2021, doi: 10.1049/rpg2.12061.

[11] A. K. Barik and D. C. Das, "Integrated resource planning in sustainable energy-based distributed microgrids," *Sustain. Energy Technol. Assessments*, vol. 48, 2021, doi: 10.1016/j.seta.2021.101622.

## 8. Appendix

System data [6], [9], [10], [11]:
$f_o = 50Hz, R_{BD} = R_{hyd} = R_{BCHP} = 2Hz/p.u.MW, M = 0.2, D = 0.01p.u.MW/Hz, K_{VA} = K_{BE} = 1,\ T_{VA} = 0.05s,\ T_{BE} = 0.05s,\ T_{RS} = 5s,\ T_{RH} = 28.75s,\ T_{HT} = 1s,\ T_{BSG} = 0.08s,\ K_R = 0.3,\ T_R = 10s,\ ,\ T_{BCT} = 0.3s,\ K_{BESS} = 1,\ \ T_{BESS} = 0.01s,\ K_N = 0.6,\ K_{FC} = 0.01,\ K_{AE} = 0.002,\ \ T_{FC} = 4s,\ T_{AE} = 0.5s,\ \ T_{WTG} = 1.5s,\ \ K_{WTG} = 1,\ \ T_{LFR} = 0.42s, K_{LFR} = 5,\ \ T_{HX} = 0.1s,\ \ K_{ORC} = 0.95, T_{ST} = 0.3s.$